A Dynamic Dual-Link Wideband MIMO Channel Sounder for 5.3 GHz

Veli-Matti Kolmonen, Peter Almers, Jussi Salmi, *Member, IEEE*, Jukka Koivunen, Katsuyuki Haneda, *Member, IEEE*, Andreas Richter, *Senior Member, IEEE*, Fredrik Tufvesson, *Senior Member, IEEE*, Andreas F. Molisch, *Fellow, IEEE*, and Pertti Vainikainen

***Abstract*—In this paper, we present and evaluate the performance of a dynamic dual-link wideband multiple-input–multiple-output (MIMO) channel sounder. The channel sounder can simultaneously measure two wideband dual-polarized links, each with a MIMO matrix size of 30 × 30 and 30 × 32. Multilink MIMO systems, including multiuser and cooperative MIMO, are essential parts of future high-throughput wireless local area networks and fourth-generation cellular systems. To fully understand such systems, the dynamic characteristics of multilink MIMO channels have to be measured. In this paper, we present a channel sounder that enables such measurements, including double-directional parameter estimation possibility for both links. The presented dual-link MIMO channel sounder does not suffer from the deficiencies of previous "virtual multiuser"measurement systems. Furthermore, system analysis and sample results from a measurement campaign with this channel sounder at 5.3 GHz in an indoor office environment are presented.**

***Index Terms*—Channel measurements, dual link, multiple-input multiple-output (MIMO), multiuser, radio channel.**

I. Introduction

WIRELESS communication has enormously grown in the recent decade. With the success of second- and third-generation mobile communication systems, wireless access has proven to be usable for reliable mobile voice and data communications, which, in turn, has increased the interest for even faster wireless connections. In theory, multiple-input–multiple-output (MIMO) systems [1]–[3] provide a solution for the ever-increasing capacity requirements and are currently being implemented into wireless local area network (WLAN) products [4] and fourth-generation cellular systems [5], [6].

The aforementioned theoretical studies are, however, based on simplified and idealized channel models. For an assessment of the true potential and performance of MIMO systems, measurements of MIMO propagation channels are a prerequisite. For this reason, there has recently been extensive research on this topic (for an overview, see [7] and [8]), and a special measurement equipment has been designed [9]–[11] for this purpose. Based on the measured transfer function matrix, the double-directional channel description [12], i.e., angular channel characteristics at the transmitter (TX) and the receiver (RX), can be extracted by sophisticated high-resolution algorithms [13], [14] to enable a detailed analysis of such channels.

The initial theoretical studies that established the benefits of MIMO dealt with a only single link. As MIMO systems are deployed, the number of multilink MIMO scenarios increases, and the need to understand the effects of multiuser interference in multilink MIMO scenarios grows. Hence, several papers have been published about the following topics: 1) MIMO systems with multiple users in a single cell (for example, see [15]–[17]); 2) the capacity of interference-limited MIMO systems without coordination [18]; and 3) interference-limited systems with base-station cooperation [19].

To fully understand the implications of multilink MIMO, measurements and models for multilink MIMO channels are required. Currently, there mostly exist only some "virtual multiuser" MIMO measurements, where several subsequently taken single-link MIMO measurements are combined to form a multilink scenario. A recent contribution [20] reports and analyzes such a measurement campaign using a single-link channel sounder; it concludes that, for measurement of some large-scale effects, a virtual multiuser approach is applicable. However, it is not valid if parts of the channel changes (e.g., due to movements of people and cars) between single-link measurements. For those situations, one needs a system that can identify the dual-link (or, more generally, multilink) channel behavior, even in time-variant channels.

In this paper, we present a dual-link wideband channel sounder that can simultaneously measure two dynamic dual-polarized links with double-directional information, each with a MIMO matrix size of 30 × 30 and 30 × 32. This channel sounder enables us to measure not only interference-limited

Manuscript received January 7, 2009; revised April 22, 2009. First published October 13, 2009; current version published March 20, 2010. This work was supported in part by the Wireless LANs With High Throughput in Interference-Limited Environments (WILATI) Project, which is a joint effort between three Scandinavian universities, and is a part of the NORDITE Research Program. The Associate Editor coordinating the review process for this paper was Dr. Jesús Ureña.

V.-M. Kolmonen, K. Haneda, and P. Vainikainen are with the Smart and Novel Radios Research Unit (SMARAD), Department of Radio Science and Engineering, Helsinki University of Technology (TKK), Espoo, Finland (e-mail: velimatti.kolmonen@tkk.fi).

P. Almers was with the Department of Electrical and Information Technology, Lund University, Lund, Sweden. He is now with Ericsson AB, Lund, Sweden.

J. Salmi is with the Department of Signal Processing and Acoustics, TKK, Espoo, Finland, and also with the University of Southern California, Los Angeles, CA USA.

J. Koivunen was with SMARAD, Department of Radio Science and Engineering, TKK, Espoo, Finland. He is now with Espotel, Espoo, Finland.

A. Richter was with the Department of Signal Processing and Acoustics, TKK, Espoo, Finland. He is now with the Nokia Research Center, Helsinki, Finland.

F. Tufvesson is with the Department of Electrical and Information Technology, Lund University, Lund, Sweden.

A. F. Molisch was with the Mitsubishi Electric Research Laboratories, Cambridge, MA USA, and also with Lund University, Lund, Sweden. He is now with the University of Southern California, Los Angeles, CA USA.

Digital Object Identifier 10.1109/TIM.2009.2026608

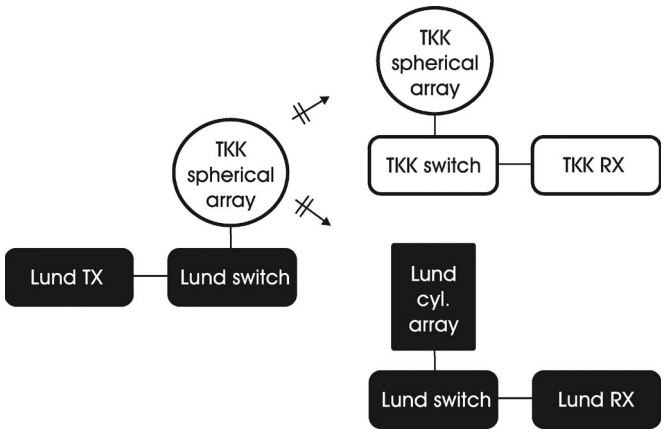

Fig. 1. Block diagram of the dual-link channel sounder setup.

MIMO links but also relay-type links. With the possibility of resolving the parameters of the multipath components in the channel, the double-directional behavior of the channel and the interference can be analyzed, and the parameters can be used in the development of multilink channel models. In addition to the work in [21]–[23], we present here a detailed system performance analysis with example results.

The remainder of this paper is organized into four sections. First, the details of the channel sounder are described, followed by an analysis of the system performance. Then, some sample results from field measurements are given, followed by a conclusion of this paper.

II. Measurement System

The dynamic dual-link MIMO channel sounder consists of two channel sounders—one from Helsinki University of Technology (TKK), Espoo, Finland, and another one from Lund University (LU), Lund, Sweden—which have appropriately been modified to work together. However, as the synchronization between the TXs could not be achieved the orthogonality between transmitted signals cannot be preserved. Therefore, the TKK TX could not be used, and hence, the channel sounder consists of LU TX and LU and TKK RXs. The measurement system can measure the dynamic point-to-multipoint and multipoint-to-point MIMO channels. Both sounders use the switched-array principle to measure the channel realization, or snapshot. In this approach, the antennas are sequentially connected through an electronic switch to a single RF chain. Due to the high speed of the electronic switch, all antenna combinations (from each TX to each RX antenna element) can be measured during a short period of time. A block diagram of the channel sounder is shown in Fig. 1. Table I shows specifications for the interoperability of the sounders. A detailed description of the channel sounders can be found in other publications [9]–[11]. Hence, here, we present only the specifications that affect the work in this paper.

A. Sounder Description

The LU sounder is a commercial RUSK wideband MIMO channel sounder that was manufactured by MEDAV GmbH [10], [11]. The TX of the LU sounder has an arbitrary waveform generator unit for generating periodic multifrequency signals with a signal period of $T_s = N \cdot 1.6\ \mu$s (see Table I). For the dual-link channel sounder, $T_s = 1.6\ \mu$s was initially chosen, because the channel sounder was planned to be used in indoor environments where the maximum excess delays are small. The transmit signal bandwidth and center frequency of the LU TX can be adjusted so that the transmitted signal can be measured with the sampling rate of the TKK RX without aliasing. The transmit signal bandwidth was selected to be 120 MHz. This bandwidth is measured during each T_s. The number of signal periods per channel can be selected to be either two or four, depending on the maximum Doppler frequency requirements. The values for the RX element switching interval, the time between MIMO snapshots, and the MIMO snapshot measurement time are shown in Table I for two and four signal periods per channel.

TABLE I
Sounder Specifications

Parameter	LU-sounder	TKK-sounder
Carrier frequency, f_c	$5150-5750$ MHz	5300 MHz
Bandwidth	$10-240$ MHz	120 MHz
TX-signal length	$1.6-25.6\ \mu$s	N/A
Sampling rate at TX	320 MHz	N/A
Sampling rate at RX	640 MHz	120 MHz
RX-element switching interval	$3.2/6.4\ \mu$s	$3.2/6.4\ \mu$s
Time between MIMO snapshots	39.322/72.090 ms	39.322/72.090 ms
MIMO snapshot measurement time	3.277/6.554 ms	3.277/6.554 ms

The fast RF switches at the TX and RX are synchronized to each other and to the transmit signal so that antenna switching occurs at the beginning of the signal period. To minimize the effect of antenna switching, a guard period is used when element switching takes place at the RX. With the guard period included, the channels between one of the antenna pairs is measured every 3.2 or 6.4 μs, depending on the number of signal periods per channel. The TX switch is a high-power switch with a maximum input power of 10W, thus enabling the channel sounder to be used for long distances. To remove the influence of the measurement system on the measurement data, a back-to-back calibration is made.

The TKK RX unit is a superheterodyne RX with a dual-channel digital sampling unit [9]. The sounder antenna switching period is adjustable and can exactly be matched with hardware changes to that of the LU sounder T_s. The antenna-switching period is synchronized with the sampling unit; hence, the correspondence between channel switching and channel samples is known. All signal processing of the received signal is performed in the postprocessing step. Hence, the postprocessing step can easily be adjusted for various types of sounding signals. The TKK RX also measures the LU TX signal in a back-to-back measurement to store the transmit signal waveform that was used in the postprocessing step. Note that the TKK RX continuously samples during the snapshot measurement, and therefore, the appropriate position of the TX signal can be selected in the postprocessing step.

B. Antenna Structures

The antennas that were used in the sounder are shown in Fig. 2. The cylindrical antenna structure that was used for the LU RX consists of four rings of 16 dual-polarized antenna elements; thus, the antenna has 64 dual-polarized (horizontal

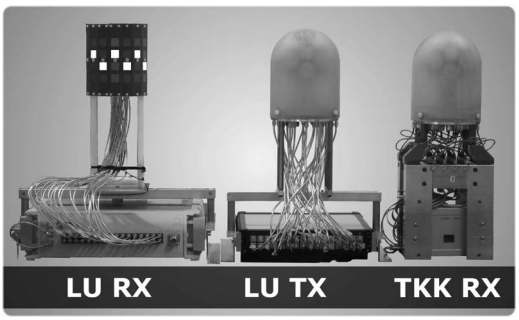

Fig. 2. Antenna structures and switches. The semispherical antennas on the right and at the center are used in the TKK RX and LU TX, respectively, and the cylindrical antenna on the left is used in the LU RX. The elements used in the LU RX are highlighted.

and vertical) antenna elements in total. Out of these dual-polarized antenna elements, 16 dual-polarized elements were used so that eight elements from each of the two middle rows were selected in an alternating fashion (see Fig. 2).

The semispherical antenna structure [9] for the TKK RX has 21 dual-polarized elements, of which the 15 lowest dual-polarized elements were connected to the switch. The semispherical antenna structure that was used for the LU TX is identical to what was used in the TKK RX, except that the polarization of the LU TX antenna elements is $\pm 45^{\circ}$ and is slanted relative to the TKK RX. In both the LU TX and the TKK RX, an omnidirectional antenna and a dummy channel for synchronization were used, in addition to the 30 channels from the dual-polarized elements. All unused antenna elements were terminated by matched loads.

C. Synchronization and Postprocessing

The sounder synchronization can be divided into the following three levels: 1) local oscillator (LO); 2) signal period and antenna switching; and 3) snapshot synchronization. In the LU sounder, all the aforementioned synchronizations exist by design, but the TKK RX operates as an unsynchronized unit for which special measures have to be taken. The synchronization of the LO and snapshot are straightforward to resolve, but the signal period T_s and antenna-switching sequence synchronization had to be resolved by hardware changes and adapting the postprocessing[1] of the measurement data. The antenna-switching synchronization is crucial for MIMO measurements to parallelize, i.e., create a MIMO measurement matrix from the serial measurement data. Furthermore, the calculation of the channel transfer function (CTF) had to be modified for the LU-TX—TKK-RX link. The required postprocessing steps are described as follows.

1) *LO synchronization*. In all nodes, the operation is synchronized either to one common 10-MHz reference or to an LO clock signal. If individual LOs are used, the TKK RX is manually tuned to the LU TX LO. The LO offset can be seen in the channel impulse response (IR) of the back-to-back system calibration measurement as an IR peak drift in the delay domain between snapshots. The TKK RX LO frequency offset is estimated from the phases of the IR peak values and is corrected during postprocessing by back or forward rotation using a complex phasor, i.e., using a mixer that was implemented in the software.
2) *Signal period extraction*. As shown in Fig. 3, the signal period starts at an arbitrary position within one of the measured TKK RX channels. This position remains constant until either sounder is shut down. Several signal periods are measured for each TX and RX channel combination. Thus, it is possible to minimize the effect of the TX switching by extracting the transmit signal period at a proper position at the RX for the channel where TX switching occurs.
3) *Channel synchronization*. The switching sequences of the LU TX switch and the TKK RX switch are not time aligned (see Fig. 3). The difference in time reference is not known in advance. However, as the antenna switching periods are exactly the same, the timing offset remains constant until either sounder is shut down.

   As shown in the figure, during each TX switching period, all N_R RX channels at the TKK RX are measured. For the TX channel connected to the matched load, this instance yields N_R inactive channels at the RX. This inactive period can be detected, e.g., using a moving average of the received power, yielding a sufficiently accurate estimate of the offset between the TX and the RX switching frame. This offset, along with TKK RX channel switching and channel samples correspondence, is used to time align the switching patterns in the postprocessing by reordering the RX channels.
4) *Snapshot synchronization*. The start of a measurement is not synchronized between the LU RX and the TKK RX. The mapping of the MIMO snapshots of the LU RX with the MIMO snapshots of the TKK RX was obtained using a switch at the LU TX. Therefore, in all of the measurements, the TX power was switched on shortly after the sampling was started at both the RXs. Using the snapshots where the power is switched on as a reference, the MIMO snapshots of the TKK RX and the LU TX could be synchronized in the postprocessing step. Due to this method, the (constant) time difference between the snapshots of the two links is always smaller than the time between MIMO snapshots in Table I.
5) *Estimation of CTF*. The raw measured data have to be postprocessed to obtain CTFs for both links. The CTF for the LU TX-RX link can be estimated from the measured data using the least squares (LS) approach [10], because the frequency response of the LU TX-RX link has a very small ripple. For the TKK RX, there is a large ripple in the frequency response at the edges of the measured bandwidth. Consequently, the LS approach cannot be used to estimate the CTF for the LU TX-TKK RX link due to significant noise enhancement at the edges. Therefore, a minimum mean square error (MMSE) solution has been applied to estimate the CTF for this link.

[1]For two signal periods per channel, the signal synchronization has to manually be checked. For four signal periods per channel, the whole postprocessing step can be automated due to the sufficient number of samples per channel.

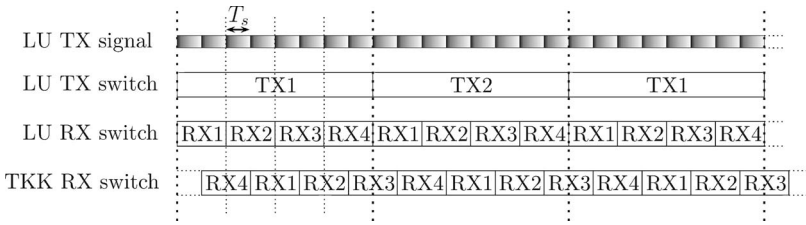

Fig. 3. Channel structure in the measurements between the LU and TKK sounders for two TX, four RX channels, and two transmit signal periods per channel. One transmit signal period is marked with T_s.

III. Measurement System Analysis and Performance

To evaluate the performance and limitations of the channel sounder, specific measurements were conducted. For all the results in this section, four transmit signals per channel were used (see Table I), and hence, the time between the CTF measurements is $4 \cdot 1.6\ \mu\text{s} = 6.4\ \mu\text{s}$. The measurements were listed as follows:

1) back-to-back measurement, where the two RXs were connected to the TX with cables and through an adjustable attenuator and a power splitter. All the included components in the back-to-back setup were separately calibrated with a vector network analyzer (VNA), and the TX output power was measured with a power meter. This measurement can be used to verify the intersnapshot synchronization, sensitivity levels, and dynamic ranges of the RXs, as well as other system nonidealities like phase noise;
2) anechoic chamber measurement, where the full channel sounder, including the switches and antennas, were placed at known positions inside an anechoic chamber. From this measurement, the absolute received powers can be determined;
3) antenna calibration measurement, where the full radiation patterns of all the elements in all antenna structures have been measured in an anechoic chamber for two polarizations, enabling the estimation of the double-directional parameters for both links.

A. Dynamic Range and Sensitivity Levels

When using the channel sounder in measurements, the dynamic ranges and sensitivity levels of the RXs have to be known. Both RXs use an active gain control (AGC), which essentially determines the dynamic range of the RX. The AGC adjusts the received power level to avoid saturation. The dynamic ranges of the two RXs are shown in Fig. 4. To avoid damaging the RXs, the input power was not increased beyond the AGC range.

P_{in} in the figure was calculated using the VNA calibration data of the back-to-back measurement chain with known output power of the LU TX. Hence, P_{in} is the input power in the RX connector. P_{out} was calculated by incoherently summing all frequency bins over a *single channel* (i.e., one T_s) out of 1024 channels. Fig. 4 indicates that the P_{out} of both RXs

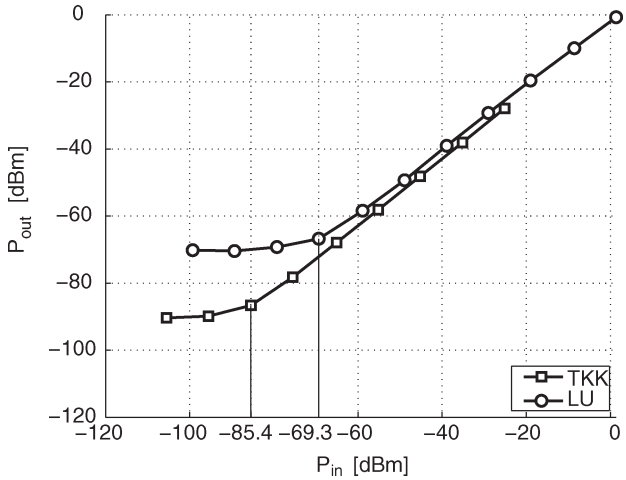

Fig. 4. Dynamic range of the RXs. The sensitivity levels are shown with vertical lines.

linearly follows the P_{in} in their dynamic range.[2] The average error between P_{in} and P_{out} in the dynamic range were 0.2 dB and 2.5 dB for the LU and TKK RXs, respectively, and are due to the calibration inaccuracies. The sensitivity levels[3] are shown in the figure with vertical lines. Interestingly, the TKK RX has a $\sim$16.1 dB lower sensitivity level than the LU RX.

B. Phase Noise

The phase noise properties of the TKK and LU channel sounders were earlier analyzed [24], [25]. However, the LU TX-TKK RX link has not yet been analyzed. Here, we evaluate the phase noise effect on a *dual-link* MIMO channel sounder in terms of the Allan variance, phase noise distribution and autocorrelation, and MIMO channel capacity with and without interference.

The demeaned phases from the back-to-back measurement within one snapshot are shown in Fig. 5(a) and (b) from the TKK and LU RXs, respectively, and the probability density functions (PDFs) and the variances of the phases are plotted in Fig. 6(a) and (b). The PDFs in Fig. 6 revealed a good fit to a Gaussian PDF, which was confirmed with the Kolmogorov–Smirnov test [26] (with a confidence level of 5%).

[2]Here, the dynamic range of the RX is referred to as the P_{in} range, i.e., between the RX saturation level (the level where the AGC is at its minimum) and the sensitivity level.

[3]Here, we refer the sensitivity level of the RX to the lowest point of P_{in}, where P_{out} is no longer linear with respect to P_{in}.

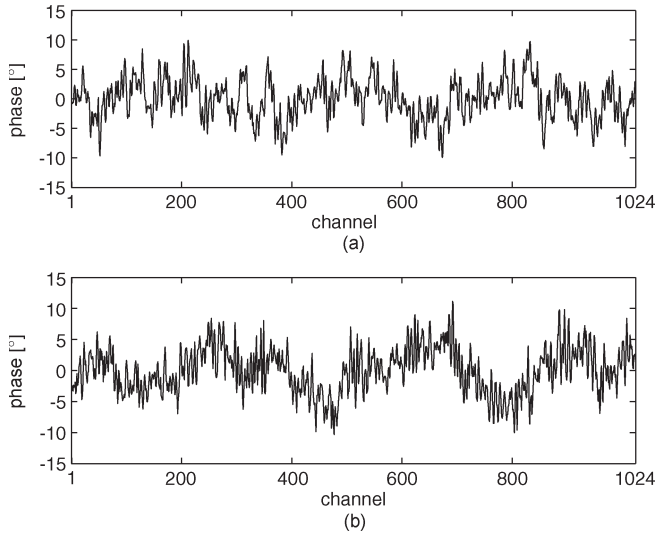

Fig. 5. Phases of the received signal from the back-to-back measurement within one snapshot from (a) the TKK RX and (b) the LU RX.

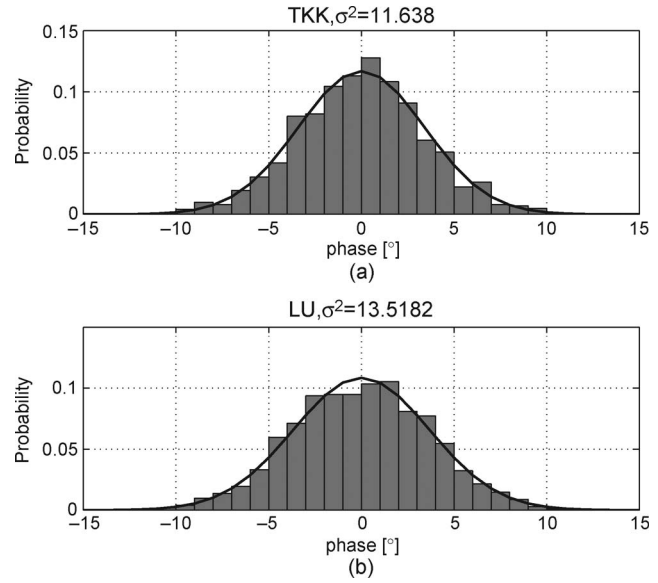

Fig. 6. PDF of the received signal phases from the back-to-back measurement within one snapshot from (a) the TKK RX and (b) the LU RX.

Ideally, the phases would be flat in Fig. 5, but the system imperfections generate small variations to the phase, i.e., the phase noise. Here, the phase samples are from the peak values of IRs, therefore we have 1024 samples within one snapshot, each corresponding to one channel.

In Fig. 7, the autocorrelation functions (ACFs) $R_{xx}(m) = E[\mathbf{x}_n \mathbf{x}^*_{n-m}]$, where $E[\cdot]$ is the expectation operator, of the phases are shown. The autocorrelation rapidly decreases, and at channels 14 and 45 for the TKK and LU RXs, the correlation is as small as 0.2. The channel time alignment by reordering the channels in the postprocessing step does not significantly change the ACF of the phases. The effect of the short-term phase correlation in Fig. 7 is shown in the Allan variance, which is defined as [27], [28]

$$\sigma_y^2(\tau) = \left\langle \frac{(\overline{y}_{k+1} - \overline{y})^2}{2} \right\rangle, \tag{1}$$

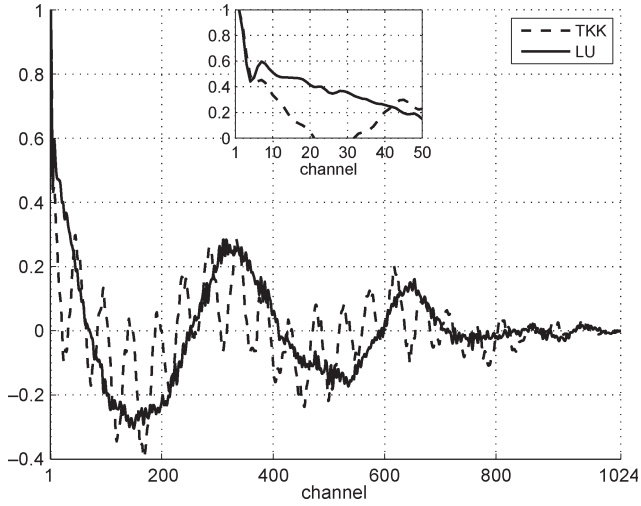

Fig. 7. Autocorrelation of the back-to-back measurement phases within one snapshot.

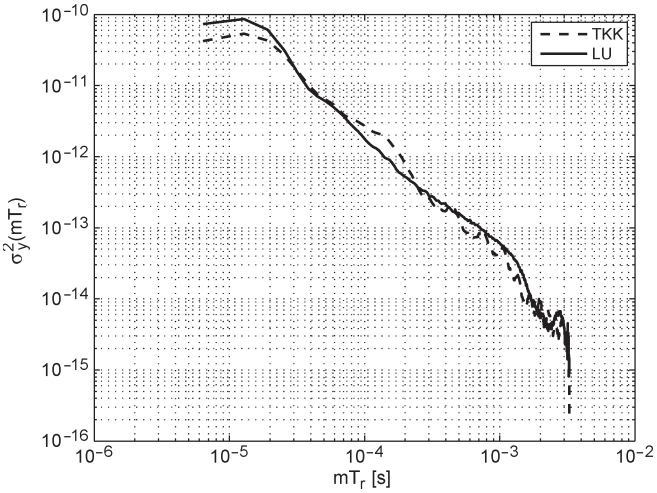

Fig. 8. Allan variance of the two links within one snapshot.

where $\langle \cdot \rangle$ is the infinite-time average, and

$$\overline{y}_k = \frac{1}{\tau} \int_{t_k}^{t_k+\tau} y(t)dt = \frac{\varphi(t_k + \tau) - \varphi(t_k)}{2\pi f_c \tau}, \tag{2}$$

where $\varphi(t_k)$ is the phase noise sample at time instant t_k, f_c is the center frequency, and $t_{k+1} = t_k + \tau$. Using $\tau = mT_r$, the Allan variance can be calculated as

$$\sigma_y^2(mT_r) = \frac{1}{2(N-2m)(2\pi f_c m T_r)^2} \times \sum_{k=1}^{N-2m} \left(\varphi(t_{k+2m}) - 2\varphi(t_{k+m}) + \varphi(t_k)\right)^2, \tag{3}$$

where N is the number of time measurements, which are spaced by T_r.

The Allan variances for the RXs using (3) are plotted in Fig. 8. The variances of the RXs are at an equal sufficiently low level compared to previous work [25]. Hence, with respect

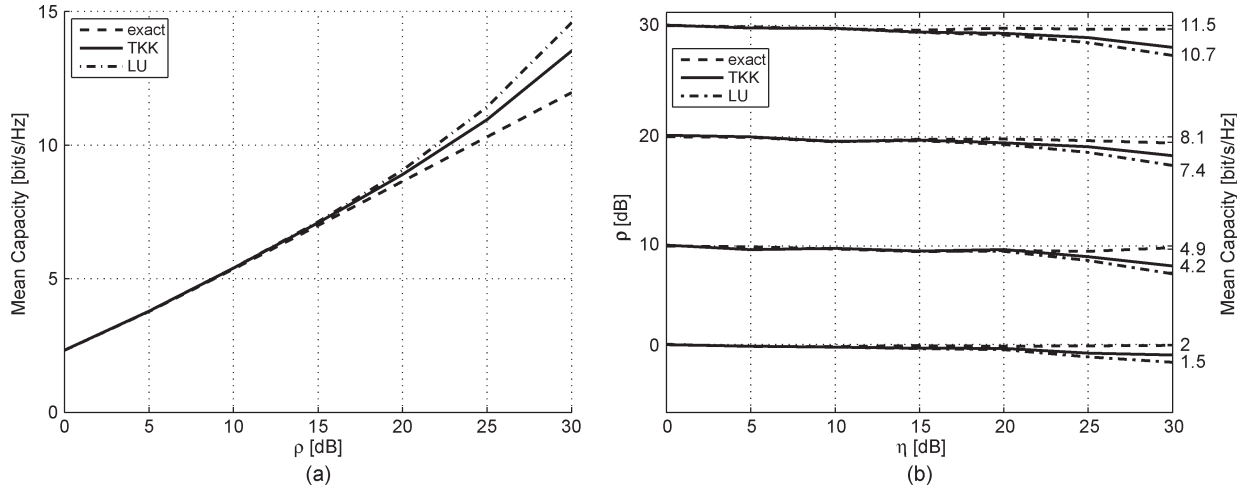

Fig. 9. Mean capacity over the frequency in the measured and simulated rank-1 channels (a) without interference and (b) with interference.

to the phase noise, the links have comparable performance, and either link can be selected as the desired or the interfering link.

C. Capacity With Phase Noise and Interference

The effect of phase noise in switched measurement systems to MIMO capacity was first analyzed in [29], where it was shown that the phase noise can lead to 100% errors in capacity estimation for high signal-to-noise ratio (SNR). In [9], [25], and [30], the effect of phase noise was analyzed for single-link channel sounders, and it has been confirmed that the capacity estimation error is clearly smaller in practical channel sounders due to correlated phase noise.

In [17], the MIMO capacity with interference is computed under the assumption that each user transmits without knowing the exact interference environment. Using the derivations in [21], we can express the capacity with interference as

$$C_k = \log_2 \left[\det \left(\mathbf{I}_{N_R} + \frac{\rho}{N_T} \mathbf{H}_{0,k} \mathbf{H}_{0,k}^{\mathrm{H}} \mathbf{R}_{\mathbf{I},k}^{-1} \right) \right] \quad (4)$$

where the instantaneous covariance matrix for our case becomes

$$\mathbf{R}_{\mathbf{I},k} = \eta_1 \mathbf{H}_{1,k} \mathbf{H}_{1,k}^{H} + \mathbf{I}_{N_R} \quad (5)$$

where $\mathbf{H}_{0,k}$ represents the channel matrix of the user of interest, and $\mathbf{H}_{1,k}$ is the interfering channel transfer matrix of the narrowband frequency subchannel k. ρ and η are the SNR and the interference-to-noise ratio, respectively, N_T is the number of transmit antennas, and $\mathbf{I}_{N_R}$ is the identity matrix of size N_R.

In Fig. 9, the mean capacity over the frequency for the simulated ("exact") rank-1 channel and measured channel from back-to-back measurements are shown for 4×4 MIMO configuration *without* and *with* interference and with varying values of ρ and η. The simulated channel matrices were produced by $\mathbf{H} = \mathbf{h}_r \mathbf{h}_t^{\mathrm{H}}$, where $\mathbf{h}_i \in \mathbb{C}^{N_R,1}$ is a zero-mean complex Gaussian random vector with a unit variance, and $(\cdot)^H$ denotes the conjugate transpose. The $\mathbf{H}$ matrices were normalized to $\|\mathbf{H}\|_F^2 = N_R \cdot N_T$, where $\|\cdot\|_F$ is the Frobenius norm [31] of a matrix. In Fig. 9(b), the selected values of ρ are shown on the left y-axis, and the capacity values are shown on the right y-axis. The exact result was calculated using simulated rank-1 channels for $\mathbf{H}_{0,k}$ and $\mathbf{H}_{1,k}$, whereas the results from the measurement were calculated using simulated $\mathbf{H}_{0,k}$ and back-to-back measured $\mathbf{H}_{1,k}$ for both RXs.

Fig. 10. Measurement environment (taken from the second-floor balcony that overlooks the atrium). The example measurement route on the third floor is shown with an arrow.

The result in Fig. 9(a) is in line with the previous work, verifying that the single-link capacity results do not suffer from the phase noise in the low-SNR region. Capacity under interference also follows the theoretical result in the low-SNR region. In the high-SNR region, the capacity is underestimated due to the phase noise.

Note that, in deriving Fig. 9, consecutive channels were used where the interchannel correlation is the highest (see Fig. 7). Therefore, it represents the lowest capacity error scenario. By selecting the channels furthest apart from each other (but equally spaced), the worst case scenario can be achieved. For the worst case, the capacity error without interference grows from 0.41 to 1.41 b/s/Hz, with $\rho = 20$ dB, and with interference, it grows from 0.17 to 0.41 b/s/Hz, with $\rho = \eta = 20$ dB.

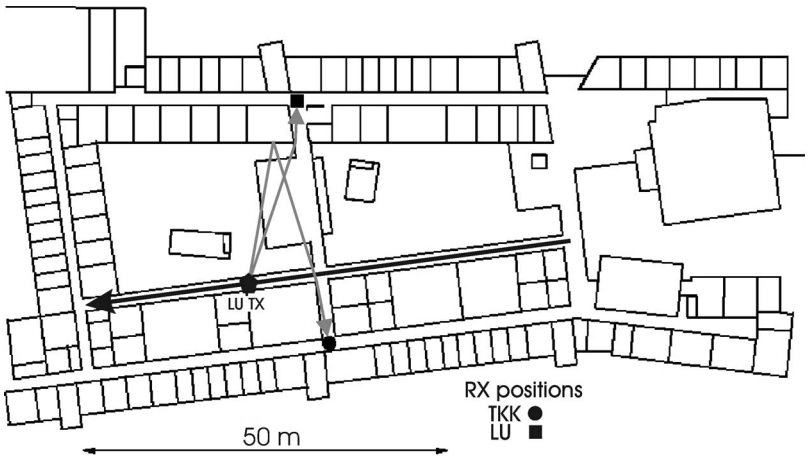

Fig. 11. Example route on the third floor. The measurement route is marked with a black arrow, and the gray arrows illustrate possible traveling paths of the waves.

IV. Measurement Campaign and Sample Results

A. Measurement Environment

The dual-link channel sounder was used in a measurement campaign in the Computer Science Building, TKK. The building is a modern three-storey office building with a large open space (60 m $\times$ 25 m) that covers all three floors in height at the center, similar in style to a shopping mall (see Fig. 10). The office walls around this center area are made of metal, bricks, plaster boards, and glass, and all the surrounding balconies have 1.2-m-high metallic rails with vertical bars. At the third floor, in addition to the rail, concrete pillars are next to the balcony edge. The outer walls of the building are made of bricks, and there are no other nearby buildings. At the second and third floors, there are bridges that cross the open space.

The LU and TKK RX antennas were positioned at the heights of 1.8 and 1.9 m, respectively, to resemble base-station or access-point positions, and the LU TX was at the height of 1.4 m, emulating a smart phone. Two transmit signal periods per channel were measured, and the time between MIMO snapshots was 39.32 ms. The speed of the TX was 0.6 m/s on the average, hence approximately 2.5 MIMO snapshots were taken per wavelength. In the measurements, the RXs were placed in several locations within the building, and the TX was moved at the center space and in the surrounding office corridors.

In the example measurement route, the RXs were placed in the second floor on the opposite sides of the open space in the office corridors, and the TX was moved along the *third* floor balcony that overlooks the open space (see Fig. 10). The measurement route is shown in Fig. 11 with a black arrow. The route covers most of the long side of the open space.

B. Results

As an example of the dual link capability of the measurement system, we show an example of correlated shadow fading found in the measurements. In addition, azimuth angles and delays of the two links are shown to illustrate the double-directional parameter estimation results. The parameter estimation results were produced with an algorithm that was described in detail in [14].

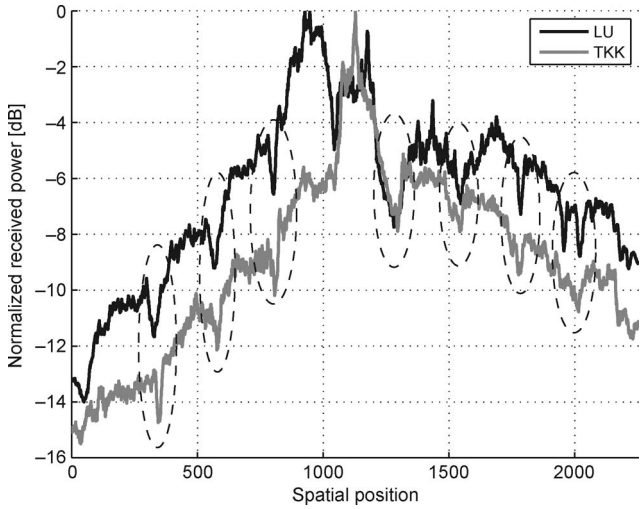

Fig. 12. Received powers for the two RXs. The power values were individually normalized in each link.

The correlated shadow fading phenomenon is highlighted in Fig. 12, where the received powers for the two links are shown. The received power was calculated by incoherently summing all of the CTFs over the frequency and antenna elements, and the individual powers of the RXs were normalized to their maximum values. The highlighted sections are approximately 7 m apart from each other, corresponding to the separation of the concrete pillars in Fig. 10.

The estimated azimuth direction of departures (DoD), direction of arrival (DoA), and delays for the measurement route for the two links are shown in Figs. 13–15, respectively. The power values were normalized to the maximum path power, and the delay values were moved to the beginning of the delay window. The results for the elevation angle are very similar to the results for the azimuth angle. The 0° azimuth direction points upward in Fig. 11, and the positive rotation direction of the azimuth angle is counterclockwise. In the figures, the paths with less than ten snapshot lifetimes[4] were removed.

[4]Here, the lifetime of a path is defined as the number of consecutive snapshots where the path is found.

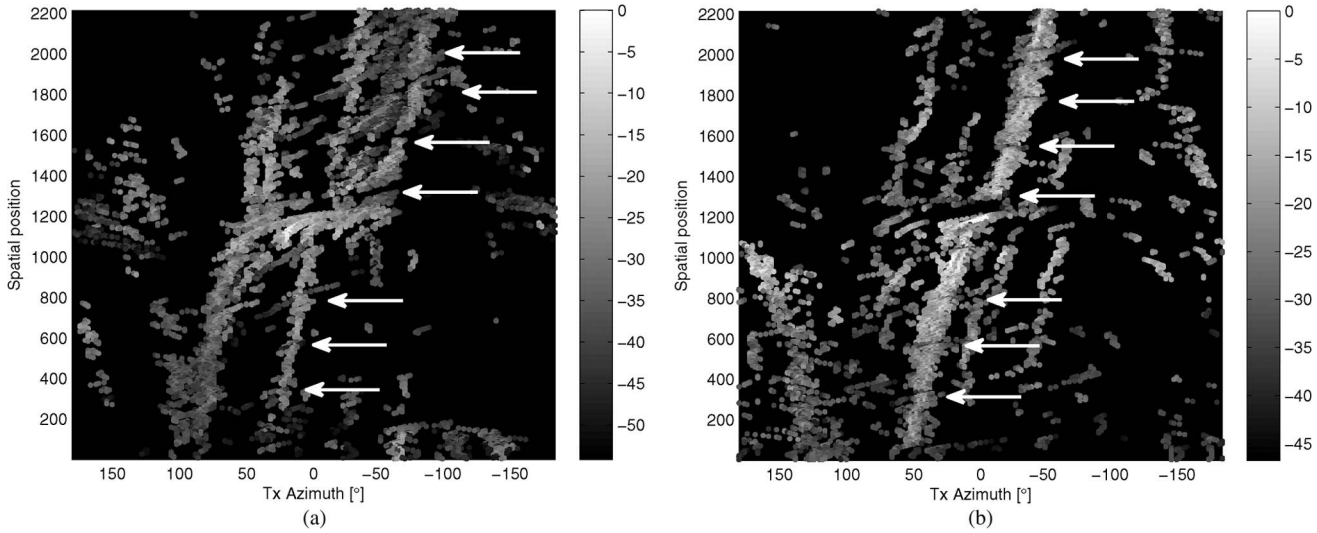

Fig. 13. Double-directional parameter estimates for the azimuth DoD for (a) the LU TX—TKK RX link and (b) the LU TX—LU RX link. The correlated shadow fading phenomenon is highlighted with arrows.

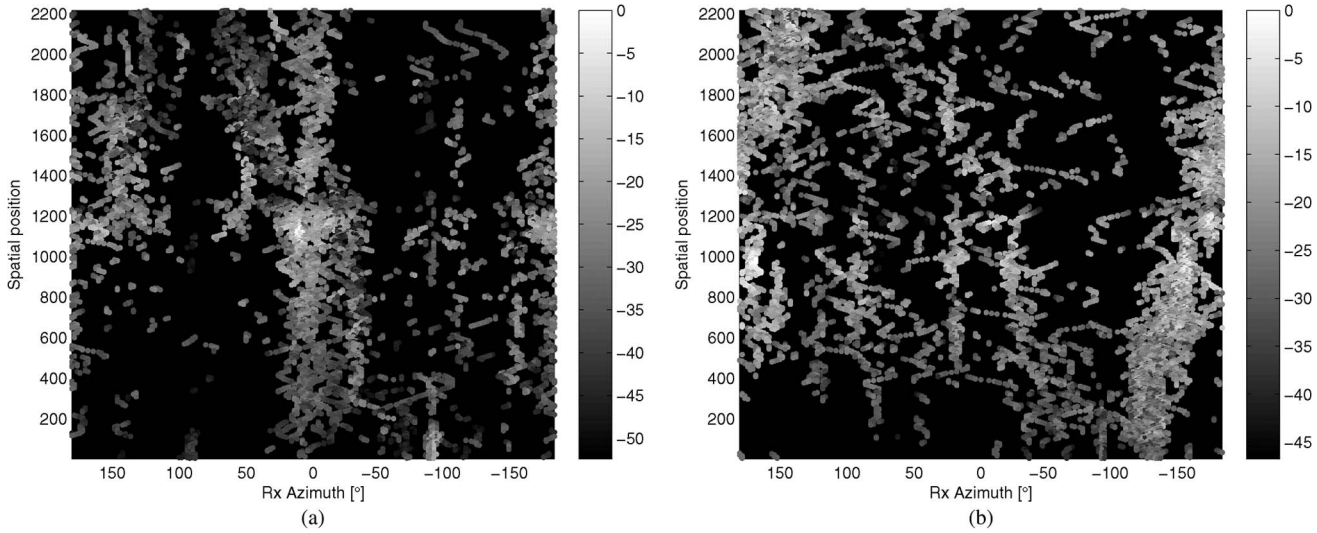

Fig. 14. Double-directional parameter estimates for the azimuth DoA for (a) the LU TX—TKK RX link and (b) the LU TX—LU RX link.

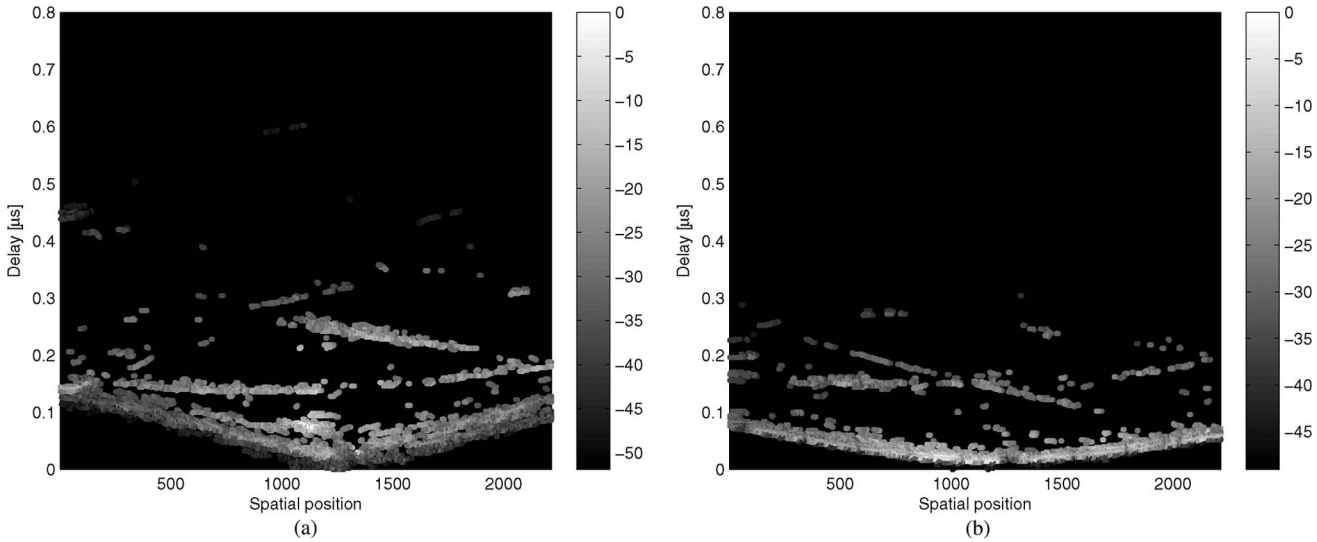

Fig. 15. Double-directional parameter estimates for the delay for (a) the LU TX—TKK RX link and (b) the LU TX—LU RX link.

The correlated shadow-fading behavior can be understood by analyzing the propagation environment and the double-directional parameter estimates. Both RXs are connected to the open space through a doorway, whereas the direct connection is being blocked by the surrounding building structures. In Fig. 13, we can see that most of the waves depart from the TX toward the open space, and the correlated fading is shown as horizontal discontinuities of the parameter estimates along the route. The discontinuities are highlighted with arrows. Hence, the waves propagate across the open space through the doorway to the LU RX while bouncing from the LU RX side's wall when traveling to the TKK RX (see the gray lines in Fig. 11). Hence, the signal paths to different RXs have a common initial traveling path, although the RXs are separated by many wavelengths. Therefore, all structures, e.g., the concrete pillars, that affect this common signal path induce a correlated behavior in the RX. The results for the RXs are much more scattered due to the surrounding building structures.

This particular case suggests that two radio links may have correlated scatterer distribution, even if terminal separation is large at the other side of the link. The characterization and modeling of such a phenomenon is crucial in the design of multilink systems. Here, the advantage of our dual-link channel sounder is obvious in order to accurately monitor the correlated shadow fading. We also note that our sounder can measure correlated scattering induced by moving scatterers, e.g., humans who shield off radiation.

V. Conclusion

We have presented a dual-link wideband channel sounder for 5.3 GHz, which can simultaneously measure two dynamic dual-polarized double-directional links, each with a MIMO matrix size of 30×30 and 30×32. The technical specifications and required modifications to the individual sounders were shown and discussed, and the developed measurement data postprocessing methods were described. Additional effort was required to synchronize the different parts of the channel sounder, and therefore, hardware and data postprocessing modifications were applied.

The performance of the system was analyzed with respect to the dynamic range, sensitivity level, and phase noise and its effect on channel capacity with and without interference. This analysis shows that this channel sounder is well suited to characterize dual-link MIMO propagation channels. Furthermore, it was shown that, with the presented modifications to the postprocessing step, a dual-link channel measurement system can be constructed using an unsynchronized equipment.

The channel sounder has been used in several measurement campaigns, and an example of the true dual-link double-directional channel characterization results have been presented for the first time.

Acknowledgment

The authors would like to thank the Finnish Cultural Foundation, the HPY Foundation, Nokia Foundation, the Swedish Strategic Research Foundation Center of Excellence for High-Speed Wireless Communications, and the Academy of Finland CoE in Smart Radios and Wireless Research Unit (SMARAD). The authors would also like to thank P. Suvikunnas and J. Poutanen for their support.

References

[1] G. J. Foschini and M. J. Gans, "On limits of wireless communications in fading environments when using multiple antennas," *Wirel. Pers. Commun.*, vol. 6, no. 3, pp. 311–335, Mar. 1998.

[2] I. E. Telatar, "Capacity of multiantenna Gaussian channels," Bell Lab., Lucent Technol., Murray Hill, NJ, Oct. 1998. Technical Memorandum.

[3] J. H. Winters, "On the capacity of radio communications systems with diversity in Rayleigh fading environments," *IEEE J. Sel. Areas Commun.*, vol. 5, no. 5, pp. 871–878, Jun. 1987.

[4] *Wireless LAN Medium Access Control (MAC) and Physical Layer (PHY) Specifications: Enhancements for Higher Throughput*, IEEE Draft Standard: 802.11n, 2007.

[5] *Local and Metropolitan Area Networks: Air Interface for Fixed Broadband Wireless Access Systems*, IEEE Pre-Draft Standard: 802.16m, 2007.

[6] Third Generation Partnership Project (3GPP), *Evolved Universal Terrestrial Radio Access (E-UTRA): Long-Term Evolution (LTE) Physical Layer*. (3GPP TS 36.201), v8.1.0. [Online]. Available: www.3gpp.org

[7] P. Almers, E. Bonek, A. Burr, N. Czink, M. Debbah, V. Degli-Esposti, H. Hofstetter, P. Kyösti, D. Laurenson, G. Matz, A. Molisch, C. Oestges, and H. Özcelik, "Survey of channel and radio propagation models for wireless MIMO systems," *EURASIP J. Wireless Commun. Netw.*, vol. 2007, no. 1, p. 56, Jan. 2007.

[8] A. F. Molisch and F. Tufvesson, "Multipath propagation models for broadband wireless systems," in *Digital Signal Processing for Wireless Communications Handbook*. Boca Raton, FL: CRC Press, 2004, pp. 2.1–2.43.

[9] V.-M. Kolmonen, J. Kivinen, L. Vuokko, and P. Vainikainen, "5.3-GHz MIMO radio channel sounder," *IEEE Trans. Instrum. Meas.*, vol. 55, no. 4, pp. 1263–1269, Aug. 2006.

[10] R. Thomä, D. Hampicke, A. Richter, G. Sommerkorn, A. Schneider, U. Trautwein, and W. Wirnitzer, "Identification of time-variant directional mobile radio channels," *IEEE Trans. Instrum. Meas.*, vol. 49, no. 2, pp. 357–364, Apr. 2000.

[11] [Online]. Available: http://www.channelsounder.de/ruskchannelsounder.html

[12] M. Steinbauer, A. F. Molisch, and E. Bonek, "The double-directional radio channel," *IEEE Antennas Propag. Mag.*, vol. 43, no. 4, pp. 51–63, Aug. 2001.

[13] B. Fleury, P. Jourdan, and A. Stucki, "High-resolution channel parameter estimation for MIMO applications using the SAGE algorithm," in *Proc. Int. Zurich Seminar Netw. Broadband Commun.*, 2002, pp. 30-1–30-9.

[14] J. Salmi, A. Richter, and V. Koivunen, "Detection and tracking of MIMO propagation path parameters using state-space approach," *IEEE Trans. Signal Process.*, vol. 57, no. 4, pp. 1538–1550, Apr. 2009.

[15] G. Caire and S. Shamai, "On the achievable throughput of a multiantenna Gaussian broadcast channel," *IEEE Trans. Inf. Theory*, vol. 49, no. 7, pp. 1691–1706, Jul. 2003.

[16] W. Yu, W. Rhee, S. Boyd, and J. Cioffi, "Iterative water filling for Gaussian vector multiple-access channels," *IEEE Trans. Inf. Theory*, vol. 50, no. 1, pp. 145–152, Jan. 2004.

[17] R. S. Blum, "MIMO capacity with interference," *IEEE J. Sel. Areas Commun.*, vol. 21, no. 5, pp. 793–801, Jun. 2003.

[18] S. Catreux, P. F. Driessen, and L. J. Greenstein, "Attainable throughput of an interference-limited multiple-input–multiple-output (MIMO) cellular system," *IEEE Trans. Commun.*, vol. 49, no. 8, pp. 479–493, Aug. 2001.

[19] G. J. Foschini, H. Huang, K. Karakayali, R. A. Valenzuela, and S. Venkatesan, "The value of coherent base station coordination," in *Proc. in Conference on Information Sciences and Systems (CISS'05)*, Mar. 2005, pp. 141–145.

[20] N. Czink, B. Bandemer, G. Vazquez-Vilar, L. Jalloul, and A. Paulraj, "Can multiuser MIMO measurements be done using a single channel sounder?" in *Proc. COST 2100 6th Manage. Committee Meeting*. Lille, France, Oct. 6–8, 2008. TD(08)621.

[21] J. Koivunen, P. Almers, V.-M. Kolmonen, J. Salmi, A. Richter, F. Tufvesson, P. Suvikunnas, A. F. Molisch, and P. Vainikainen, "Dynamic multilink indoor MIMO measurements at 5.3 GHz," in *Proc. EuCAP*, Edinburgh, U.K., Nov. 2007, pp. 1–6.

[22] A. Richter, F. Tufvesson, P. S. Rossi, K. Haneda, J. Koivunen, V.-M. Kolmonen, J. Salmi, P. Almers, P. Hammarberg, K. Pölönen, P. Suvikunnas, A. F. Molisch, O. Edfors, V. Koivunen, P. Vainikainen, and R. R. Müller, "Wireless LANs with high throughput in interference-limited environments: Project summary and outcomes," in *Proc. COST 2100 5th Manage. Committee Meeting*, Wroclaw, Poland, Feb. 6–8, 2008. TD(08)432.

[23] P. Almers, K. Haneda, J. Koivunen, V.-M. Kolmonen, A. F. Molisch, A. Richter, J. Salmi, F. Tufvesson, and P. Vainikainen, "A dynamic multi-link MIMO measurement system for 5.3 GHz," in *Proc. 29th URSI Gen. Assembly*, Chigaco, IL, Aug. 2008.

[24] J. Kivinen and P. Vainikainen, "Phase noise in a direct-sequence-based channel sounder," in *Proc. 8th IEEE Int. Symp. PIMRC: Waves of the Year 2000*, Sep. 1–4, 1997, vol. 3, pp. 1115–1119.

[25] P. Almers, S. Wyne, F. Tufvesson, and A. F. Molisch, "Effect of random-walk phase noise on MIMO measurements," in *Proc. IEEE VTC—Spring*, 2005, vol. 1, pp. 141–145.

[26] F. J. Massey, "The Kolmogorov–Smirnov test for goodness of fit," *J. Amer. Stat. Assoc.*, vol. 46, no. 253, pp. 68–78, Mar. 1951.

[27] J. A. Barnes, A. R. Chi, L. S. Cutler, D. J. Healey, D. B. Leeson, T. E. McGunigal, J. A. Mullen, W. L. Smith, R. L. Sydnor, R. F. Vessot, and G. M. Winkler, "Characterization of frequency stability," *IEEE Trans. Instrum. Meas.*, vol. IM-20, no. 2, pp. 105–120, May 1971.

[28] F. Walls and D. W. Allan, "Measurements of frequency stability," *Proc. IEEE*, vol. 74, no. 1, pp. 162–168, Jan. 1986.

[29] D. Baum and H. Bolcskei, "Impact of phase noise on MIMO channel measurement accuracy," in *Proc. IEEE VTC—Fall*, Los Angeles, CA, Sep. 26–29, 2004, vol. 3, pp. 1614–1618.

[30] A. Taparugssanagorn, J. Ylitalo, and B. Fleury, "Phase noise in TDM-switched MIMO channel sounding and its impact on channel capacity estimation," in *Proc. IEEE GLOBECOM*, 2007, pp. 4559–4564.

[31] G. Golub and C. V. Loan, *Matrix Computations*, 3rd ed. Baltimore, MD: The Johns Hopkins Univ. Press, 1996, p. 694.

Veli-Matti Kolmonen received the M.Sc. degree in technology from Helsinki University of Technology (TKK), Espoo, Finland, in 2004.

Since 2003, he has been with the Smart and Novel Radios Research Unit (SMARAD), Department of Radio Science and Engineering, TKK, first as a Research Assistant and later as a Researcher. His research interests include radio channel measurements and modeling.

Peter Almers received the M.S. degree in electrical engineering and the Ph.D. degree in radio systems [through a scholarship from TeliaSonera AB (formerly Telia AB), Malmö, Sweden] from Lund University, Lund, Sweden, in 1998 and 2007, respectively.

In 1998, he was with the Radio Research Department, TeliaSonera AB, where he mainly worked on WCDMA physical-layer issues and as a 3GPP WG1 Standardization Delegate. He has participated in the European research initiative European Cooperation in Scientific and Technical Research (COST) 273, the European Network of Excellence in Wireless Communications (NEWCOM), and was involved in the NORDITE project Wireless LANs With High Throughput in Interference-Limited Environments (WILATI). He was a Research Fellow with the Department of Electrical and Information Technology, Lund University. He is currently with Ericsson AB, Lund, Sweden.

Dr. Almers is the recipient of the IEEE Best Student Paper Award at the 13th International Symposium on Personal, Indoor, and Mobile Radio Communications (PIMRC 2002).

Jussi Salmi (S'05–M'09) was born in Finland in 1981. He received the M.Sc. and D.Sc. degrees (both with honors) from Helsinki University of Technology (TKK), Espoo, Finland, in 2005 and 2009, respectively.

From 2004 to 2005, he was a Research Assistant with the Radio Laboratory, TKK, where he has been a Researcher with the Department of Signal Processing and Acoustics since 2005. He is currently a Visiting Postdoctoral Research Associate with the University of Southern California, Los Angeles. His research interests include measurement-based MIMO channel modeling, parameter estimation, analysis of interference-limited multiuser MIMO measurements, tensor modeling, and decomposition techniques.

Dr. Salmi was the recipient of the Best Student Paper Award at the Fourth European Signal Processing Conference (EUSIPCO 2006) and a corecipient of the Best Paper Award in Propagation at the First European Conference on Antennas and Propagation (EuCAP 2006).

Jukka Koivunen is currently working toward the M.Sc. degree in technology at Helsinki University of Technology (TKK), Espoo, Finland.

From 2005 to 2007, he was a Research Assistant with the Radio Laboratory, TKK, where he was involved in projects on 5- and 60-GHz MIMO and multilink MIMO channel measurements and participated in the development of the channel measurement equipment, channel measurements, and postprocessing of the measurement data. Since 2008, he has been with Espotel, Espoo, as a DSP Software Testing Engineer and a Software Developer.

Katsuyuki Haneda (S'03–M'07) received the Dr.Eng. degree from Tokyo Institute of Technology, Tokyo, Japan, in 2007.

Since 2007, he has been a Postdoctoral Researcher with the Smart and Novel Radios Research Unit (SMARAD), Department of Radio Science and Engineering, Helsinki University of Technology (TKK), Espoo, Finland. His research interests include radio-wave propagation measurements and modeling, UWB radio, and multiple-input–multiple-output systems.

Mr. Haneda is a member of the Institute of Electronic, Information and Communication Engineers, Japan. He is the recipient of the Best Student Paper Award at the Seventh International Symposium on Wireless Personal Multimedia Communications (WPMC 2004).

Andreas Richter (M'04–SM'08), was born in Germany in 1969. He received the Dipl.Ing. (M.Sc.) degree in electrical engineering and the Dr.Ing. (Ph.D.) degree (*summa cum laude*) from the Technische Universität Ilmenau, Ilmenau, Germany, in 1995 and 2005, respectively.

From 1995 to 2004, he was a Research Assistant with the Electronic Measurement Laboratory, Technische Universität Ilmenau. From July to October 2001, he was a Guest Researcher with the Wireless Laboratories, NTT DoCoMo Inc., Yokosuka, Japan. From 2004 to 2008, he was a Senior Research Fellow with the Statistical Signal Processing Laboratory, Department of Signal Processing and Acoustics, Helsinki University of Technology (TKK), Espoo, Finland. Since August 2008, he has been a Principal Member of Research Staff with the Nokia Research Center, Helsinki, Finland. He has published more than 70 peer-reviewed papers in international scientific conference proceedings and journals. His research interests include digital communication, sensor arrays, and statistical signal processing.

Dr. Richter was the recipient or a corecipient of the Best Paper Award at the Fourth European Mobile Communications Conference (EPMCC 2001), 2004 International Symposium on Antennas and Propagation (ISAP), 16th IEEE International Symposium on Personal, Indoor and Mobile Radio Communications (PIMRC 2005), Fourth European Signal Processing Conference (EUSIPCO 2006), and First European Conference on Antennas and Propagation (EuCAP 2006). He received the Siemens Communications Academic Award in 2005 and, with his former colleagues at the Technische Universität Ilmenau, the Thuringian Research Award for Applied Research in 2007 for their work on MIMO channel sounding.

Fredrik Tufvesson (S'97–A'00–M'04–SM'07) was born in Lund, Sweden, in 1970. He received the M.S. degree in electrical engineering, and the Licentiate and Ph.D. degrees from Lund University, Lund, in 1994, 1998, and 2000, respectively.

After almost two years with the startup company Fiberless Society, he is currently an Associate Professor with the Department of Electrical and Information Technology, Lund University. His research interests include channel measurements and modeling for wireless communication, in particular channels for both MIMO and UWB systems, as well as channel estimation and synchronization problems, OFDM system design, and UWB transceiver design.

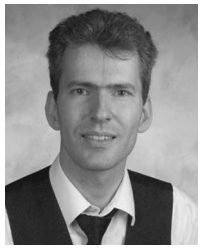

Andreas F. Molisch (S'89–M'95–SM'00–F'05) received the Dipl.Ing., Dr.Techn., and habilitation degrees from the Technical University of Vienna, Vienna, Austria, in 1990, 1994, and 1999, respectively.

He was with the AT&T (Bell) Laboratories Research, Middletown, NJ, Lund University, Lund, Sweden, the Mitsubishi Electric Research Laboratories, Cambridge, MA, and the Technical University of Vienna, Vienna, Austria. He is currently a Professor of electrical engineering with the University of Southern California, Los Angeles, CA. He is the author, a coauthor, or an Editor of four books, including the textbook *Wireless Communications* (Wiley-IEEE Press), 11 book chapters, more than 120 journal papers, and numerous conference contributions, as well as more than 70 patents and 60 standards contributions. His research interests include the measurement and modeling of mobile radio channels, UWB, cooperative communications, and MIMO systems.

Dr. Molisch is a Fellow of the IET and an IEEE Distinguished Lecturer. He was the General Chair, the Technical Program Committee Chair, or the Symposium Chair of several international conferences and the Chair of various international standardization groups. He has received several awards.

Pertti Vainikainen received the M.Sc. (Tech.), Lic.Sc. (Tech.), and Dr.Sc. (Tech.) degrees from Helsinki University of Technology (TKK), Espoo, Finland, in 1982, 1989, and 1991, respectively.

From 1992 to 1993, he was an Acting Professor of radio engineering with the Radio Laboratory (now the Department of Radio Science and Engineering), TKK, where he became an Associate Professor of radio engineering in 1993 and has been a Professor of radio engineering since 1998. From 1993 to 1997, he was the Director of the Institute of Radio Communications (IRC), TKK. He was a Visiting Professor with Aalborg University, Aalborg, Denmark, in 2000 and with the University of Nice, Nice, France, in 2006. He is the author or a coauthor of six books or book chapters and about 300 refereed international journal papers and conference proceedings. He is the holder of 11 patents. His research interests include antennas and propagation in radio communications and industrial measurement applications of radio waves.